Computer-Aided Design 190 (2026) 103977

Contents lists available at ScienceDirect

Computer-Aided Design

journal homepage: www.elsevier.com/locate/cad

Research Paper

Topo-GenMeta: Generative design of metamaterials based on diffusion model with attention to topology

Liang Du [a,1], Jiangbei Hu [a,b,1], Shengfa Wang [a,*], Yu Jiang [a,c], Na Lei [a], Ying He [b], Zhongxuan Luo [a]

[a] School of Software, Dalian University of Technology, China
[b] College of Computing and Data Science, Nanyang Technological University, Singapore
[c] Department of Mechanical and Aerospace Engineering, The University of Manchester, UK

ARTICLE INFO

Keywords:
Metamaterial
Topology-aware
Persistent homology
Denoising diffusion probabilistic model

ABSTRACT

Metamaterials are a family of artificial materials that achieve unique properties by designing the shape of unit cell structures. Expanding the metamaterial unit cell library is a key focus in this field, with the aim of enhancing the design flexibility to meet multifunctional requirements across diverse physical scenarios. Recent advancements in data-driven generative techniques using deep learning have significantly sped up innovations in metamaterial design. However, existing approaches mostly focus on the geometric characteristics of unit structures without considering their topological properties explicitly, which we believe are essential for enhancing design diversity and enriching material properties. In this study, we propose a novel data-driven metamaterial design methodology that combines the denoising diffusion probabilistic model with the persistent homology technique. Our model is capable of generating high-fidelity and functionally effective unit structures. Furthermore, by incorporating topological properties derived from persistent homology into the diffusion process, our method facilitates the generation of a diversity of metamaterial unit structures with richer shapes and properties. To the best of our knowledge, this is the first approach to explicitly consider topological properties in metamaterial design. In addition, our method also supports multi-scale design applications, enabling the generation of metamaterial units that align with the desired properties to achieve the optimization objectives.

1. Introduction

Metamaterials are artificial engineered materials designed to exhibit effective properties beyond those found in nature [1,2], enabling advancements across various fields, including optics, acoustics, aerospace, mechanical engineering, and biomedicine [3–6]. Rather than discovering new material compositions, metamaterials achieve their special properties through the design of unit cell structures with specific geometric and topological configurations. In recent years, advances in computer science and additive manufacturing technology have led to significant progress in the practical engineering applications of metamaterials [7,8]. The question of how to design reasonable and novel metamaterials has become a widely concern among researchers. Early metamaterials design methods relied on empirical knowledge [9]. Later, more mature approaches adopted parametric design strategies that confine metamaterials to a limited range of selectable properties [10]. However, these methods encounter significant challenges, such as matching unit cell structures with their effective properties across multiple scales and navigating numerous local optima in the design optimization process. Their primary limitation lies in restricted design flexibility. Expanding the metamaterial library as broadly as possible is essential for meeting application demands across various fields, particularly in extreme environments.

The application and rapid development of artificial intelligence in engineering have opened up vast possibilities for metamaterial design [11,12]. Numerous data-driven methods have been developed [13], advancing metamaterial design through efficient design space exploration. By leveraging deep learning models, these approaches enable rapid exploration of large-scale design spaces, facilitating the discovery of high-performance or novel structures. Data-driven methods for metamaterial design encompass three primary components: First, a dataset of unit cell structures is required, typically containing structural representations and corresponding physical properties. Subsequently, a neural network-based machine learning surrogate module extracts

* Corresponding author.
E-mail address: sfwang@dlut.edu.cn (S. Wang).
[1] Equal contribution.

https://doi.org/10.1016/j.cad.2025.103977
Received 23 June 2025; Received in revised form 20 August 2025; Accepted 19 September 2025
Available online 10 October 2025

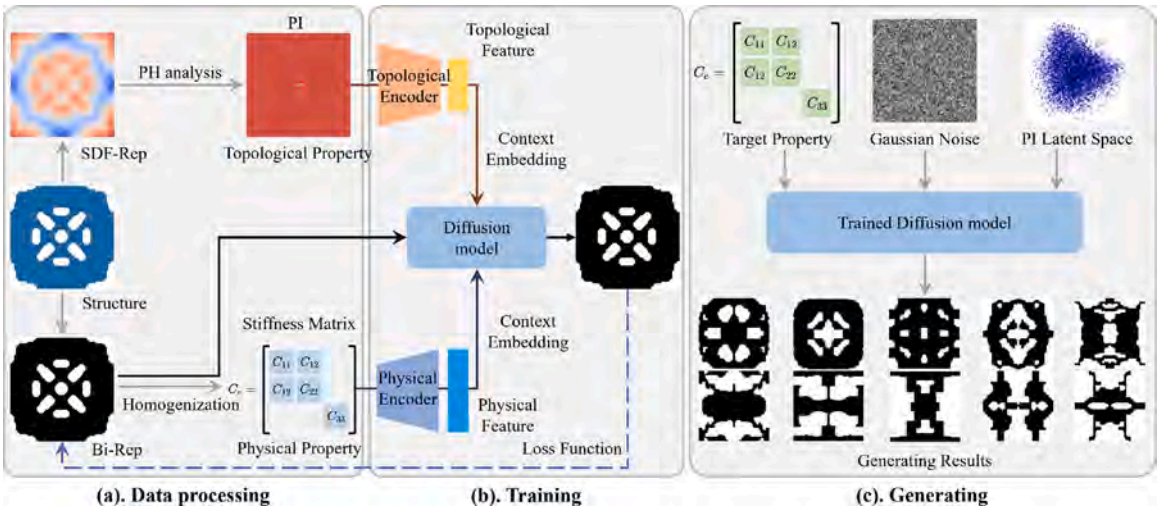

Fig. 1. Pipeline. (a) Our dataset comprises unit structures of metamaterials with two representations: SDF-Rep and Bi-Rep, along with their physical and topological properties. (b) We train a DDPM-based generative model to reconstruct these unit structures (Bi-Rep), conditioning on their physical and topological properties. (c) Our framework enables the generation of unit metamaterial structures with diverse shapes and properties.

features from the data to facilitate unit cell designs. Finally, the unit cell database and machine learning models are integrated to generate metamaterials with desired properties across multi-scales, from the microscopic level of individual unit cells to the macroscopic level of the assembled structure. The most commonly used network models in this field are deep generative models, such as Variational Autoencoders (VAEs) [14,15] and Generative Adversarial Networks (GANs) [16]. However, while VAEs are simple and efficient, they often suffer from poor reconstruction accuracy, leading to low-quality structures that fail to achieve the desired physical properties. Additionally, the diversity of novel metamaterial structures generated by VAEs remains limited. Although GANs can generate high-quality and diverse unit cells, their adversarial training process is unstable and prone to model collapse, which undermines the model's reliability. Moreover, most existing data-driven methods capture structural features by focusing only on local geometric characteristics, such as treating unit cell structures as images and encoding them using CNNs [17]. The global topological characteristics of a structure influence its performance and function, yet this has not been directly considered in existing metamaterial design related work.

In this paper, we propose a novel framework, *Topo-GenMeta*, to design metamaterials with an attention to topological features (see Fig. 1). Our method enables topology-aware generation by combining the Denoising Diffusion Probabilistic Model (DDPM) and the Persistent Homology (PH) technique. Specifically, we first prepare a dataset of unit cell structures, each represented in two formats: a discrete binary representation (Bi-Rep) and a continuous signed distance function representation (SDF-Rep). Using the Bi-Reps, we calculate the physical properties of each unit structure through the homogenization method. In this work, we focus on the stiffness matrix, but our approach can be extended to other general properties. Meanwhile, we extract the topological properties of the unit structures from the SDF-Reps by applying PH analysis. Next, we train a self-supervised DDPM to reconstruct the Bi-Reps of structures. To enhance control over the generation process, we introduce a conditioning mechanism that guides the diffusion process based on physical properties, topological features, or a combination of both. Once trained, the diffusion model enables the generation of novel metamaterial unit structures through sampling. Our method supports specifying physical property conditions to generate metamaterials with desired properties. By explicitly incorporating topological characteristics, it enables the generation of metamaterial unit structures with highly diverse shapes and physical properties. This expands the solution space for macroscopic material design, further enhancing the application potential of metamaterials. Extensive conducted experiments demonstrate that our framework not only generates high-quality, effective metamaterials but also excels in enhancing diversity in both shape and properties. Our method successfully generates structures beyond the original dataset with varying stiffness, negative Poisson's ratio, wave propagation, and biomedical properties, showcasing its versatility across different functional requirements.

We summarize our contributions as follows:

- We propose a novel metamaterial design framework that explicitly incorporates topological features by leveraging persistent homology.
- Our method remarkably enhances metamaterial design diversity through joint exploration of geometric and topological feature spaces.
- Our method not only generates high-quality, valid structures but also discovers diverse new properties beyond the original dataset.

2. Related work

2.1. Data-driven metamaterial design

Recent progress in designing metamaterials through data-driven approaches has shown impressive results. The creation of tailored neural architectures has notably sped up the inverse design procedure. Early works used CNNs as encoder–decoder frameworks to predict the design of 2D metamaterials with target mechanical properties [17–19]. CNN-based methods are constrained by resolution limitations, resulting in poor generalizability and design diversity. Later research applied VAEs to encode structures into a structured latent space, thereby enhancing the efficiency of design exploration [14]. However, VAEs tend to fall short in the quality of both reconstructed and generated metamaterials. For specific material behaviors, cGANs were developed using Voronoi-based datasets to achieve controllable generation of auxetic metamaterials [16]. Graph neural networks (GNNs) further extended these capabilities by combining VAE with property predictors, creating behaviors [20]. Some innovations incorporate physical constraints and multi-network architectures to enhance design precision. Physics-informed networks enabled the inverse design of anisotropic truss structures for bone implants [21], while multi-network systems facilitated the design of gradient metamaterials by prediction of parallel properties [22]. The advent of diffusion models has notably propelled the prediction of

nonlinear deformations, as demonstrated by the high performance of video diffusion frameworks [23] and DiffMat [24] in scenarios involving substantial strains. Moreover, specialized models for metamaterials with curved beams have successfully managed the concurrent control of Poisson's ratio alongside dimensional constraints [25].

One of the primary objectives of metamaterial design is to expand the metamaterial library, enabling more efficient exploration and discovery of novel structures with tailored properties. This, in turn, facilitates their applications in diverse engineering fields. METASET [26] pioneered data-driven unit cell selection through similarity metrics and determinantal point processes, improving structural diversity. This was extended by t-METASET [15], which integrated active learning with generative shape descriptors to optimize dataset acquisition efficiency. Recent work [27] incorporating guided diffusion models aims to address boundary consistency issues in metamaterials generative design while covering a broader range of elastic properties. Nevertheless, current approaches focus solely on geometric characteristics when creating metamaterial structures, a limitation we assert hindering the diversification process. For the first time, we integrate topological features into the design of metamaterial unit cells by utilizing persistent homology techniques.

2.2. Persistent homology

The performance of a structure is influenced by both its geometric characteristics, including size and thickness [28], and its topological attributes, such as holes and connections [29,30]. Persistent homology (PH) is a powerful tool for extracting topological characteristics from complex data [31–33]. PH has showcased successful applications in various machine learning-related fields, which can significantly enhance data analysis and pattern recognition capabilities [34–36]. Moor et al. proposed a topological autoencoder aimed at preserving the topological features of the input data in low-dimensional representations [37]. In the biomedical field, PH has found the most widespread applications [38–40]. In recent years, PH has also been used in the field of computer graphics to enhance traditional point clouds and 3D geometric representations [41–43]. The development of topologically-aware neural networks based on PH [44] has been greatly advanced by technologies that convert PH analysis results into vectorized information, such as persistence landscape [45], Betti curve [46], and persistence images [47].

In structural engineering, topology-based techniques leveraging PH have also been gaining increasing attention. Lin et al. utilized PH to analyze and construct porous structures [48,49]. Behzadi et al. were the first to suggest the use of a PH-based topological loss to enhance structural continuity [50]. Hu et al. proposed an end-to-end topology optimization framework, which incorporates a topological loss based on PH to improve the accuracy of the prediction [51]. In this work, we aim to develop a topology-aware diffusion model based on PH, enabling metamaterial unit cell design to incorporate both geometric and topological features, thereby enhancing the diversity of structural design.

3. Preliminary

3.1. Denoising diffusion probabilistic model

The probabilistic denoising diffusion model mainly comprises two phases, *i.e.*, a forward diffusion process and a reverse denoising process. We briefly introduce the principles of DDPM in this section; refer to [52] for more details.

Forward diffusion process. Given a sample from a certain distribution $x_0 \sim q(x)$, the forward process can be understood as a fixed Markov chain which adds Gaussian noise at each time step t,

$$q(x_t|x_{t-1}) = \mathcal{N}(x_t; \sqrt{1-\beta_t}x_{t-1}, \beta_t I), \tag{1}$$

where $\beta_t \in (0,1)$ is a variance schedule. We can sample x_t at any time step t: $q(x_t|x_0) = \mathcal{N}(x_t; \sqrt{\bar{\alpha}_t}x_0, (1-\bar{\alpha}_t)I)$, via setting $\alpha_t = 1-\beta_t$, $\bar{\alpha}_t = \prod_{i=1}^{t}\alpha_i$. And the sample can be given by $x_t = \sqrt{\bar{\alpha}_t}x_0 + \sqrt{1-\bar{\alpha}_t}\epsilon$ with $\epsilon \sim \mathcal{N}(0, I)$.

Reverse denoising process. To obtain the original data by a denoising process, we approximate this probability distribution with a neural network, denoted as

$$p_\theta(x_{t-1}|x_t) = \mathcal{N}\left(x_{t-1}; \mu_\theta(x_t, t), \Sigma(x_t, t)\right), \tag{2}$$

where $\mu_\theta(x_t, t)$ is the predicted mean and $\Sigma(x_t, t)$ is set to a constant. $\mu_\theta(x_t, t)$ can be decoupled into two terms relating to x_t and ϵ_θ. Specifically, the formulation is $\mu_\theta(x_t, t) = \frac{1}{\sqrt{\alpha_t}}\left(x_t - \frac{\beta_t}{\sqrt{1-\bar{\alpha}_t}}\epsilon_\theta(x_t, t)\right)$, ϵ_θ is commonly a neural network to learn the added noise, where θ are learnable parameters.

3.2. Persistent homology analysis

Persistent homology (PH) aims to extract multi-scale topological features from original data filtered by a real value function, i.e., filtration function. We introduce the main concepts used in our study below; please refer to [32] for more details.

Given that we represent unit cells of metamaterial as a spatial aggregate of solid/void elements, it is direct to select the use of a cubical complex [53,54] to perform the PH analysis. A cubical complex is regarded as a discretization of its underlying space, which is suitable for handling grid-like data such as images and voxels. For the dth chain group $\mathbb{C}_d(\mathcal{K})$ of a cubical complex $\mathcal{K}$, we define the dth cycle group $\mathbb{Z}_d = \mathrm{Ker}\partial_d = \{\sigma \in \mathbb{C}_d \mid \partial_d\sigma = 0\}$ and the dth boundary group $\mathbb{B}_d = \mathrm{Im}\partial_{d+1} = \{\sigma \in \mathbb{C}_d \mid \exists\hat{\sigma} \in \mathbb{C}_{d+1},\ s.t.,\ \sigma = \partial_{d+1}\hat{\sigma}\}$, where $\partial_d : \mathbb{C}_d \to \mathbb{C}_{d-1}$ is the boundary operator satisfy that $\partial_0 = 1$ and $\partial_{k-1}\partial_k = 0$. The dth *homology group* is the quotient group $\mathbb{H}_d = \mathbb{Z}_d/\mathbb{B}_d$. The *Betti number* β_d is defined as the rank of $\mathbb{H}_d$ as $\beta_d = \mathrm{rank}(\mathbb{H}_d) = \mathrm{rank}(\mathbb{Z}_d) - \mathrm{rank}(\mathbb{B}_d)$, which indicates discrete topological features, such as the number of connected components (β_0), loops (β_1), and voids (β_2).

The key concept of PH analysis is the filtration process, which generates a sequence of topological spaces at different scales. Based on the filtration value function, we define a series of filtered complexes as $\mathcal{K}^i = \{\sigma \in \mathcal{K} \mid S(\sigma) \le s_i\}$, where s_i is the corresponding threshold. Therefore, by gradually increasing the filtration value, we can obtain a nested sub-complexes sequence $\emptyset \subset \mathcal{K}^0 \subseteq \mathcal{K}^1 \subseteq \cdots \subseteq \mathcal{K}^N = \mathcal{K}$. Then we represent the p–persistent dth homology group at filtration value s_i as $\mathbb{H}_d^{i,p} = \mathbb{Z}_d^i/(\mathbb{B}_d^{i+p} \bigcap \mathbb{Z}_d^i)$, where $\mathbb{Z}_d^i = \mathbb{Z}_d(\mathcal{K}^i)$, $\mathbb{B}_d^i = \mathbb{B}_d(\mathcal{K}^i)$. The p-persistent dth Betti number $\beta_d^{i,p}$ of $\mathcal{K}^i$ is the rank of $\mathbb{H}_d^{l,p}$.

For the lth n-dimensional topological feature, it corresponds to a pair (b_l^n, d_l^n), where b_l^n and d_l^n are the birth and death filtration values, respectively. The value $|d_l^n - b_l^n|$ indicates the persistence of the topological feature, which gives a geometric measurement of the topological invariant. We can represent the topological features by their birth and death pairs in a persistence diagram (PD) denoted as $\mathcal{D}$, where the pairs of points are embedded into $\mathbb{R}^2$. By examining the PD, one can easily determine the scale of the topological features (i.e., their persistence). Points closer to the diagonal indicate shorter durations of the corresponding topological features in the homology sequence, and they are likely to be identified as noise points.

Persistence diagrams are challenging to be used directly in machine learning algorithms due to their set-like structure and infinite dimensionality. Persistence images [47] offer a vectorization method that transforms PDs into a pixel-based representation. This transformation involves placing a Gaussian distribution at each point in the PD and summing these distributions over a pixel to produce an image. Such images facilitate the extraction of topological features by conventional neural networks, such as CNNs.

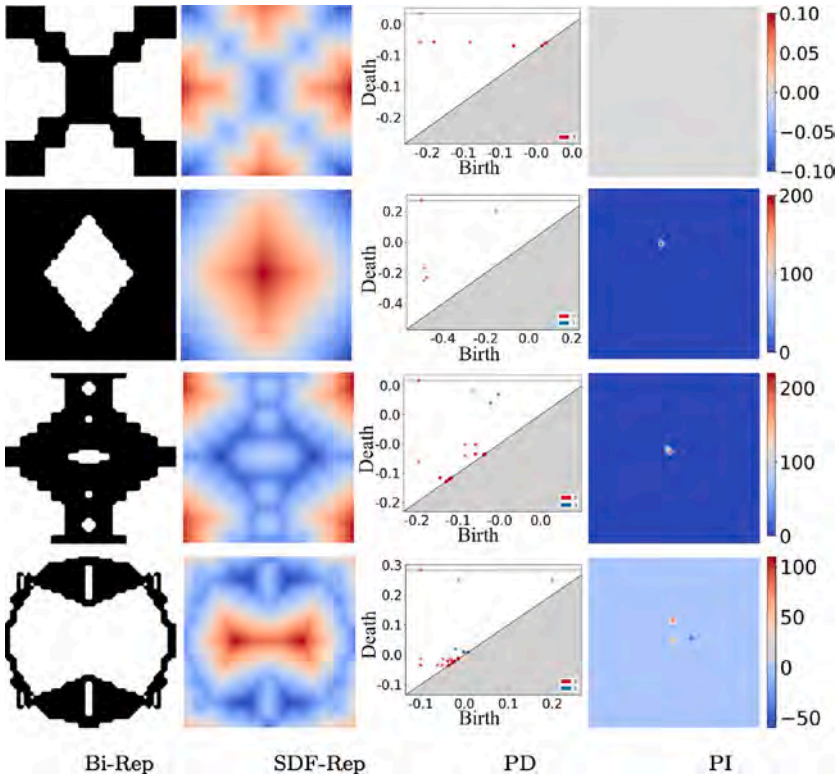

Fig. 2. Illustration of our metamaterials dataset. Each metamaterial unit cell is represented as a binary field (Bi-Rep). We compute its signed distance field representation (SDF-Rep) to derive persistence diagrams (PDs), which capture the topological properties of the structure. Finally, each PD is transformed into a persistence images (PIs), serving as input for our generative model.

4. Method

Overview. First, we prepare a 2D metamaterial dataset consisting of structural representations, physical properties, and topological features. Then, we train a denoising diffusion probability model to reconstruct the unit cell structures. In addition, we integrate physical properties and topological features into the training process using the condition mechanism. Finally, we can generate unit cell structures with high diversity and accuracy by sampling in the learned distribution.

4.1. Data preparation

4.1.1. Unit cell structures

Following the work [14], we prepare a dataset composed of a large number of 2D unit structures of metamaterials. As illustrated in Fig. 2, we represent each unit structure in two distinct representations. One is a discrete binary pixel field, referred to as *Bi-Rep*, where "1" indicates a solid pixel (black) and "0" indicates a void pixel (white). The other is a continuous signed distance field, referred to as *SDF-Rep*, indicating the shortest distance from each pixel to the nearest boundary pixel. Positive values signify pixels outside the structure, while negative values denote internal pixels.

4.1.2. Physical properties

Within our framework, we aim to discern the relationship between structural and functional properties via network learning, facilitating automated generation of metamaterial structures to target properties. Therefore, we also prepare the physical properties of all unit structures. Without loss of generality, we focus on the stiffness characteristics of the unit structure. Based on the Bi-Rep, we employ the energy homogenization algorithm [55] to calculate the stiffness matrix for each unit structure. Given that the unit structures in our dataset are orthotropic, the homogenized elastic tensor is formulated as

$$\mathbf{C} = \begin{pmatrix} C_{11} & C_{12} & 0 \\ C_{12} & C_{22} & 0 \\ 0 & 0 & C_{33} \end{pmatrix}. \tag{3}$$

The property of each unit structure is determined by four independent components: $C_{11}, C_{12}, C_{22}, C_{33}$. Our framework can be readily extended to other physical property design tasks. In the experiments, besides stiffness, we also evaluate the diversity of generated structures in terms of wave propagation, biomedical properties, and negative Poisson's ratio. The Poisson's ratio is computed based on the elastic tensor obtained according to Eq. (3) as following [56]:

$$\nu_{xy} = \frac{C_{21}}{C_{22}}, \quad \nu_{yx} = \frac{C_{12}}{C_{11}}. \tag{4}$$

4.1.3. Topological properties

Existing metamaterials datasets are limited to providing information on the geometric properties of unit structures. In contrast, our approach employs persistent homology (see Section 3.2) to extract the topological properties corresponding to each unit structure. We then integrate the topological properties into the learning of our generative model, thereby enhancing its generative diversity. We use the signed distance field (SDF-Rep) of each structure as the filtration input for persistent homology analysis. The analysis process is illustrated in Fig. 3. Given a unit structure, we compute its SDF-Rep and apply filtration by gradually increasing the SDF threshold. During this process, topological features such as connected components and loops appear and disappear. Each feature is associated with a birth value and a death value. These (birth, death) pairs form the persistence diagram (PD), where more persistent features lie farther from the diagonal. However, the results of persistent homology analysis are inherently discrete, expressed as isolated (birth, death) pairs. Such discrete points are not directly suitable for deep learning frameworks. The PD is therefore converted into a fixed-size persistence image (PI), following Adams et al. [47], which provides a stable and effective way to represent

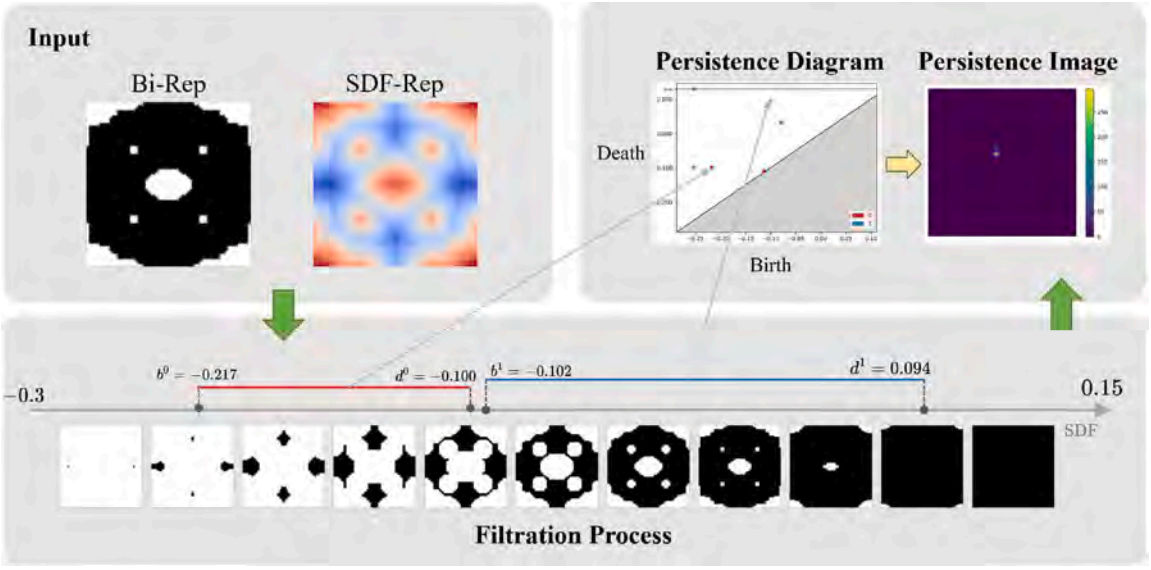

Fig. 3. Illustration of persistent homology analysis. Taking the SDF-Rep of unit structures as filtration values, we utilize the cubical complex to perform the persistent homology analysis for extracting topological properties. We utilize the persistence diagrams to depict the multi-scale topological features, where each point indicates the birth value and death value of the corresponding topological feature, respectively.

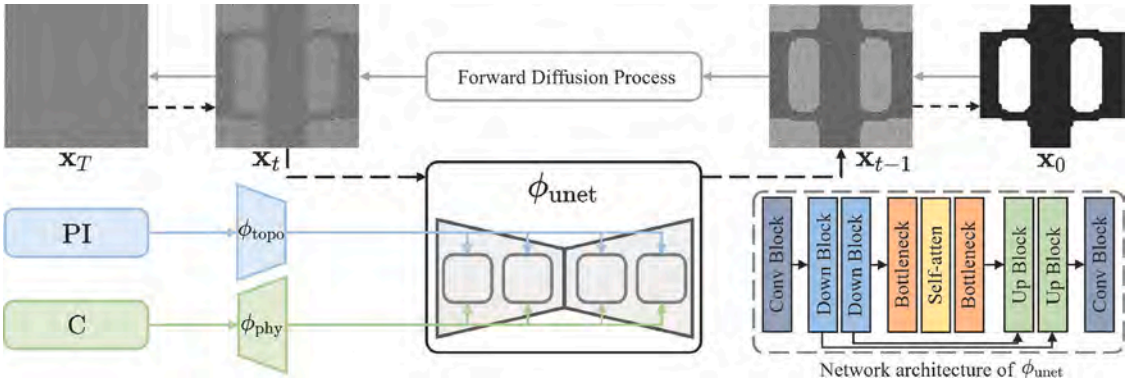

Fig. 4. The network architecture of DDPM module.

topological features in a continuous form and enables smooth integration into our generative model. In 2D structures, 1-dimensional PD points indicate the quantity and persistence of connected components, while 2-dimensional points illustrate the quantity and persistence of holes. Considering that we focus solely on unit structures with a single connected component, we convert the 2-dimensional PDs into PIs with a resolution of 64 × 64 to serve as the topological properties of the structure. For the generated results, we use 1-dimensional PD points to examine whether the structure consists of a single connected component. Structures with multiple connected components are considered failure cases. In our implementation, we utilize the GUDHI library [57] to perform persistent homology analysis to obtain topological information. It should be noted that topology and geometry are not strictly decoupled in this representation; for example, variations in thickness can affect persistence values. Nevertheless, for enhancing structural diversity, persistence-based features provide a sufficiently meaningful characterization of topology.

4.2. Topo-GenMeta framework

We build our Topo-GenMeta framework based on the DDPM module (Section 4.2.1), which incorporates physical and topological properties through a conditional mechanism during training (Section 4.2.2).

4.2.1. DDPM module

As detailed in Section 4.2.1, DDPM encompasses both a forward diffusion process and a reverse denoising process. As illustrated in Fig. 4, we gradually add noise to the Bi-Rep of the initial unit structure x_0, resulting in the eventual generation of nearly Gaussian noise x_T after T iterations. In order to reconstruct the original Bi-Rep of unit structures, which are 2D tensors, we choose to use a denoising network ϵ_θ based on U-Net [52]. Fig. 4 illustrates the network architecture, which consists of downsampling blocks, bottleneck blocks, and upsampling blocks.

4.2.2. Integrating physical and topological properties

Our generative model can randomly generate a large number of diverse unit structures with high accuracy and details, as seen in Fig. 5(b). However, it is necessary to introduce a conditional mechanism if users want to create unit structures with specific shapes or properties. We introduce the topological features and physical properties of the stiffness matrix as conditional information to guide DDPM training. Topological information is mainly used to alter the shape and topology of generated structures, thus augmenting their diversity and functionality. The components of stiffness matrix, as physical information, are used to facilitate the network produce unit structures with ideal properties. It should be noted that the stiffness matrix can be replaced by other physical characteristics, as long as a suitable encoding method can be found to introduce physical properties into network training

as conditional encoding. As described in Section 4.1.3, we represent the topological features of unit structures as persistence images (PIs), which are 2D tensors. Therefore, we employ a topological encoder τ_θ, which is a shallow CNN, to encode each PI into a 1-dimensional latent code $\mathbf{c}_{\text{topo}} \in \mathbb{R}^{L_t}$. Subsequently, we integrate the topological conditions into the main network utilizing context embedding mechanism. In our experiments, we set $L_t = 128$.

Given that physical information is the stiffness matrix of each unit structure, which consists of four independent components, as introduced in Section 4.1.2. Previous work [51] demonstrated that deep neural networks tend to learn lower frequency functions, which may limit their ability to accurately fit data with high frequency variation. Taking inspiration from NeRF [58] in the field of computer vision, we map each component of the physical properties $c \in \mathbb{R}$ into a higher dimensional space $\mathbb{R}^{2k}$ using an encoding function as

$$\gamma(c) = [\sin(2^0\pi c), \cos(2^0\pi c), \dots, \sin(2^{k-1}\pi c), \cos(2^{k-1}\pi c)], \tag{5}$$

where we set $k = 6$ in our experiments. Consequently, we obtain the embed physical information $[\gamma(c_{11}), \gamma(c_{12}), \gamma(c_{22}), \gamma(c_{33})] \in \mathbb{R}^{2k\times 4}$, which is incorporated into the main network following the same integration approach described as topological conditions. Prior to this, a physical encoder ϕ_{phy}, which is a shallow MLP, is employed to encode the physical information into a 1 dimensional latent code $\mathbf{c}_{\text{phy}} \in \mathbb{R}^{L_p}$. In our experiments, we set $L_p = 128$. During training, we utilize a probabilistic approach to mask conditional inputs to enhance robustness. Each condition, physical and topological, has a default masking probability of 0.3 in our studies. This approach allows the model to infer structures based on just physical, just topological, or both types of properties, leading to versatile conditional generation results as shown in Section 5.

4.2.3. Training and generating

Loss functions. During the training process, we use the Mean Squared Error (MSE) between the noise predicted by the model and the real noise as the loss function to optimize the parameters of our network,

$$\mathcal{L}(\Theta) = \mathbb{E}_{\mathbf{s},\epsilon\sim\mathcal{N}(0,\mathbf{I}),t}[\|\epsilon - \epsilon_\Theta(\mathbf{s}_t, t)\|], \tag{6}$$

where t is the randomly selected time step, ϵ is the real noise sampled from the standard normal distribution $\mathcal{N}(0, \mathbf{I})$, ϵ_Θ is the predicted noise. The detailed training procedure is outlined in the Algorithm 1.

Sampling. In the sampling generation phase, the fixed DDPM leverages a reverse diffusion process to produce novel structures following the training process. We employ the strategy proposed by DDIM [59] to improve sampling efficiency. Initiating with a sample from $\mathcal{N}(0, \mathbf{I})$, the process involves a sequence of reverse steps that gradually denoise the sample, thus converting the noise into a unit structure that resembles the training data in terms of distribution. At the same time, we can specify physical and topological properties to guide the generation of ideal unit structures. For topological information, CNN encodes the topological properties in a continuous space P, allowing us to randomly sample topological conditions within P to enhance the diversity of shapes and functions. The detailed generating procedure is described in the Algorithm 2

Algorithm 1: Training of Topo-GenMeta.

Input: GT Bi-Reps, PIs and physical properties of unit cells structures: $\{\mathbf{s}^i_{\text{Bi}}\}_{i=1}^N, \{\mathbf{s}^i_{\text{topo}}\}_{i=1}^N, \{\mathbf{s}^i_{\text{phy}}\}_{i=1}^N$
Output: The optimal network parameters: $\Theta^* = \{\Theta^*_{\text{unet}}, \Theta^*_{\text{topo}}, \Theta^*_{\text{phy}}\}$ and PI latent space: $\mathcal{P} = \{\mathbf{c}^j_{\text{topo}}\} \subset \mathbb{R}^{128}$.
Initialize the network ϕ_{unet}, ϕ_{topo}, ϕ_{phy}, and time steps $\mathcal{T}$
while *not converged* **do**
  Divide the dataset into M batches $\{\mathcal{D}_i\}_{i=1}^M$
  foreach *batch* $\mathcal{D}_i$ **do**
    Initialize $\mathcal{L}^i = 0$
    foreach *sample* $\mathbf{s}_j$ *in* $\mathcal{D}_i$ **do**
      $t^j \leftarrow$ sample from Uniform($\{1, \dots, \mathcal{T}\}$)
      $\epsilon^j \leftarrow$ sample from $\mathcal{N}(0, I)$
      $\mathbf{x}^j_t \leftarrow$ corrupt $\mathbf{s}^j_{\text{Bi}}$ according to t^j and ϵ^j
      $\mathbf{c}^j_{\text{topo}} \leftarrow$ encode $\mathbf{s}^j_{\text{topo}}$ via topological encoder ϕ_{topo}
      $\mathbf{c}^j_{\text{phy}} \leftarrow$ encode $\mathbf{s}^j_{\text{phy}}$ via physical encoder ϕ_{phy}
      $\hat{\epsilon}_j \leftarrow$ predict noise via Unet $\phi_{\text{unet}}(\mathbf{x}^j_t, t^j, \mathbf{c}^j_{\text{topo}}, \mathbf{c}^j_{\text{phy}})$
      $\mathcal{L}^i \leftarrow$ compute loss between ϵ^j and $\hat{\epsilon}^j$
    end
    Update Θ by $\frac{\partial \mathcal{L}^i}{\partial \Theta}$;
  end
end

5. Experiments and results

Given the experimental settings (Section 5.1), we first analyze the performance of our method on the mainly focused stiffness property, evaluating the quality, property fidelity, and diversity of generated structures (Section 5.2). Then, we extend our analysis to other applications considering various properties (Section 5.3), including the surface-to-volume ratio relevant to biomedical fields, wave propagation properties in acoustics, and the generation of negative Poisson's ratio structures. Finally, to demonstrate the applicability of our method to multiscale macroscopic structure design, we present a case where unit structures are generated to achieve target deformations (Section 5.4).

5.1. Settings

Our metamaterial dataset contains 249396 samples, each similar to that shown in Fig. 2. We train our Topo-GenMeta model with batch size configured to 512. For each epoch, 80% of the samples were randomly selected for training, while the remaining 20% were used for validation. We use the Adam optimizer with an initial learning rate of 1e−3, and reduce the learning rate by 0.1 every 50 epochs. Our network reaches stable convergence during training.

To demonstrate the advancement of our method, we compare it with the previous VAE-based DDMD (Data-Driven Metamaterials Design) methods [14,15], including VAE-Bi and VAE-SDF. Both methods employ VAE to map unit structures into a low-dimensional, continuous latent space. The distinction is in the input: binary representation and SDF representation. Specifically, we use a combination of MSE and KL divergence as the loss function, with their weights as hyperparameters: 1 and 1e−3 for VAE-Bi, and 1 and 1e−4 for VAE-SDF. The trained decoder is capable of generating unit structures from a Gaussian distribution. For the timing cost, we take approximately 27 h on one Nvidia A40 GPU during training process. And generation time for 100 structure is approximately 4 s during inference using Nvidia GeForce RTX 4090 (24 GB memory) for diffusion sampling with 100 timesteps.

Algorithm 2: Generating structures via Topo-GenMeta.

Input: Target physical properties: $\mathbf{s}^j_{\text{phy}}$; PI latent space: $\mathcal{P}$; Optimal network parameters: $\Theta^* = \{\Theta^*_{\text{unet}}, \Theta^*_{\text{topo}}, \Theta^*_{\text{phy}}\}$
$x_T \leftarrow$ sample from $\mathcal{N}(0, I)$
$\mathbf{c}^j_{\text{topo}} \leftarrow$ sample from $\mathcal{P}$
for *t from T to* 1 **do**
  $\mu, \Sigma \leftarrow \phi_{unet}(\mathbf{x}_t, t, \mathbf{c}^j_{\text{topo}}, \mathbf{s}^j_{\text{phy}}; \Theta^*_{\text{unet}})$
  $\mathbf{x}_{t-1} \leftarrow$ sample from $\mathcal{N}(\mu, \Sigma)$
end
return x_0

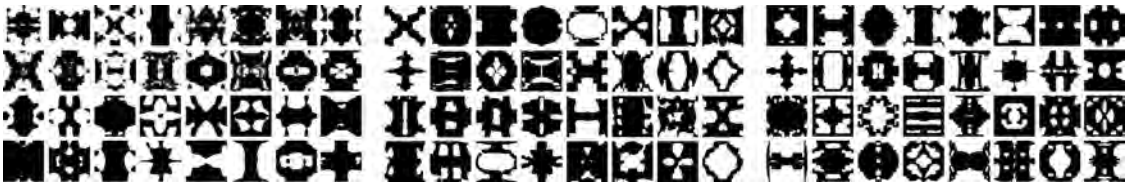

(a) VAE-based (b) GAN-based (c) Ours

Fig. 5. Comparison of generated unit structures. (a) Unit structures generated by a VAE trained on Bi-Rep dataset (top two rows) and SDF-Rep dataset (bottom two rows). (b) Unit structures generated by a GAN trained on Bi-Rep dataset (top two rows) and SDF-Rep dataset (bottom two rows). (c) Randomly generated unit structures by Topo-GenMeta: without (top two rows) and with (bottom two rows) topological properties. Our method generates structures with not only higher quality but also greater diversity.

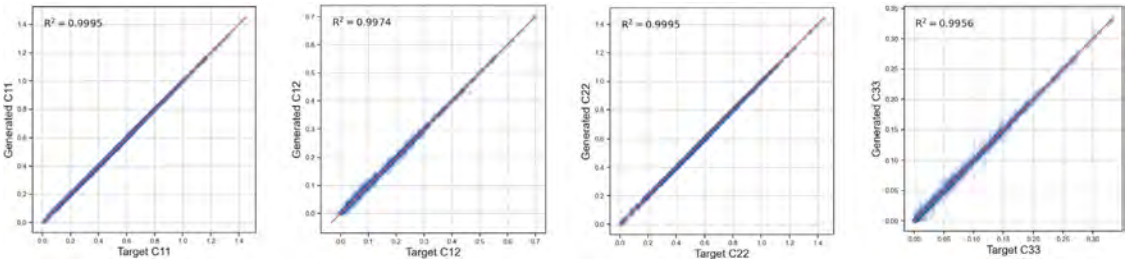

Fig. 6. The R^2 – score illustrates the disparity between the properties of the unit cells generated by Topo-GenMeta and target properties.

5.2. Performance

Structural quality. Our proposed method, Topo-GenMeta, effectively reconstructs unit structures from the training dataset and generates novel, high-quality unit structures, capturing even fine details of local features, as illustrated in Fig. 5. Our method excels at producing unit structures with clearer and more accurate boundaries, rarely resulting in floating materials. The presence of floating material indicates potential breakage and discontinuity, signaling that the structure is a failed and unusable example. Therefore, we quantify the proportion of floating material in the structures, denoted as P_{FM}, as a key metric for evaluating the performance of different methods. As shown in Table 1, the structures generated by our method exhibit the highest integrity and continuity, with the majority being fully usable.

Property fidelity. To assess the property fidelity of the unit structures generated by Topo-GenMeta according to specified physical properties, we conduct the generation process by fixing the target properties while perturbing the noise and topological features. Specifically, we randomly select 1000 sets of physical properties from the dataset and generate n unit structures for each set. Homogenization methods [55] are then employed to compute the effective properties of these generated structures. We quantify the concordance between the target and generated physical properties using the coefficient of determination(R^2 – score):

$$R^2 = 1 - \frac{\sum_{i=1}^{N} \left\| y_i - y_i' \right\|^2}{\sum_{i=1}^{N} \left\| y_i - \bar{y}_i \right\|^2}, \tag{7}$$

where y_i denotes the target physical property(C_{11}, C_{12}, C_{22}, or C_{33}), y_i' represents the actual physical property of the generated unit structures and $\bar{y}_i$ is the mean value of the target physical property. $N = 1000 \times n$ denotes the total number of generated unit structures across all property sets. To examine the impact of the number of generated unit structures on the metrics, we set $n = 4$ and $n = 10$ respectively in our experiments. We observe that the R^2 – score for both $n = 4$ and $n = 10$ is greater than 0.99, achieving high fidelity for each independent component of the stiffness matrix. Considering the highly similar results for both two cases, we have chosen to only display the results for $n = 10$ to save space, as shown in Fig. 6. This demonstrates that our method can effectively generate unit structures with accurate ideal properties.

Diversity. In the denoising phase of our Topo-GenMeta framework, we generate a structure by denoising an input Gaussian noise, guided by topological and physical properties. We can regard the noise space as the geometric feature space, and the latent space encoded by the topological encoder ϕ_{topo} as the topological feature space. Our framework can generate metamaterial unit structures with diverse shapes and properties by applying different operations in these two feature spaces:

(1) Interpolation in the geometrical feature space. Interpolation is a common technique in deep generative models to generate data with diversity and is also used to evaluate whether the feature space learned by the generative model is compact and effective. Given two source unit cells $\mathbf{s}_1$ and $\mathbf{s}_2$, we gradually add noise through the forward process, resulting in two noise data, $\mathbf{x}_1$ and $\mathbf{x}_2$, which are taken as geometric feature codes. Subsequently, we decode the feature code obtained from spherical linear interpolation, $\mathbf{x}' = \frac{\sin((1-\lambda)\theta)}{\sin\theta}\mathbf{x}_1 + \frac{\sin(\lambda\theta)}{\sin\theta}\mathbf{x}_2$, where $\theta = \cos^{-1}(\mathbf{x}_1 \cdot \mathbf{x}_2)$ and $\lambda \in [0, 1]$. By varying λ, we can obtain different interpolated unit structures with various shapes and physical properties. In Fig. 7(a), we present an interpolation example between two unit structures with low and high volumes, which are similar in shape, demonstrating a smooth transition in both shape and physical properties. To explore more complex cases, we interpolate between two unit cells with significantly different morphologies (Fig. 7(b)), We also observe the changes in the interpolation results through the Young's modulus-relative density relationship, as shown in Fig. 8. The results demonstrate smooth transitions in both shapes and physical properties between two structures.

(2) Joint exploration of the geometric and topological feature spaces. To demonstrate that our framework effectively learns the geometric and topological features of structures from the noise and topological spaces, we utilize the noise of one structure as the geometric feature input and the topological features (*i.e.* PI) of another structure as conditional guidance. As shown in Fig. 9, the generated structures are similar in both shape and topology. Furthermore, we randomly sample noise from Gaussian noise $\mathcal{N}(0, 1)$ to obtain different geometric features while using a fixed topological features of a specific structure as conditional guidance. As illustrated in Fig. 10, our generative model produces a series of structures with similar topological features but various geometric shapes. Therefore, we can enhance the diversity of generated structures by jointly sampling in the geometric and topological feature spaces. Fig.

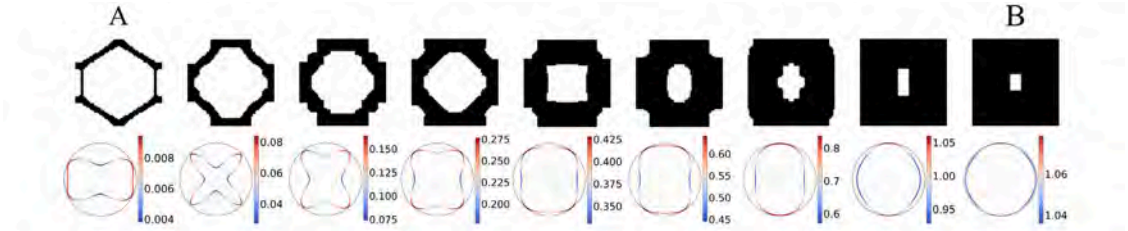

(a) Interpolated from structure A to structure B.

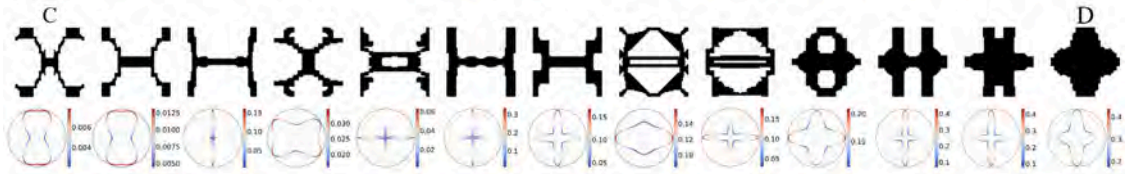

(b) Interpolated from structure C to structure D.

Fig. 7. Our framework can generating diverse unit structures with varying physical properties (illustrated by polar plot of Young's modulus) through interpolation in the geometric feature space.

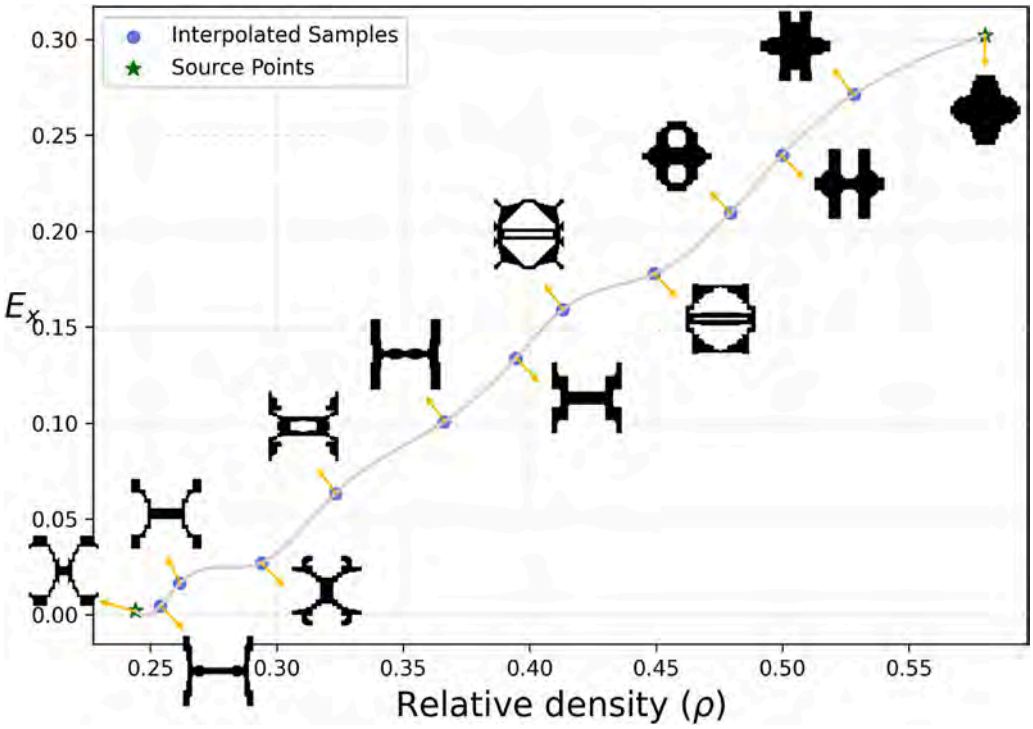

Fig. 8. We observed relatively smooth interpolation results between two significantly different shapes, both in terms of morphology and properties, with the latter reflected by the relationship between Young's modulus (E) and relative density (ρ).

11 shows the unit structures generated under random geometric feature input and random topological feature conditions.

Considering both geometric and topological features enables our model to produce metamaterial unit structures with more diverse physical properties. The 1-dimensional topological feature β_1 of a unit structure, which is actually the number of holes, can affect properties such as volume, mechanical strength, wave characteristics, and biological properties. Therefore, we use β_1 as a metric to measure topological diversity. Following the work of METASET [26], we utilize the $\det(\mathbf{L}^p)$ metric to evaluate the diversity in terms of physical properties of the generated unit structures. Specifically, we first randomly generate a set of unit structures and calculate the stiffness matrix $\mathbf{C}$ for each structure. We represent the four independent components of $\mathbf{C}$ as a vector $\mathbf{v} = (C_{11}, C_{12}, C_{22}, C_{33})^\top$ to characterize the physical property. Next, we obtain the Euclidean distance of the physical vectors between two structures as $d(i,j) = \sqrt{(\mathbf{v}_i - \mathbf{v}_j)^\top(\mathbf{v}_i - \mathbf{v}_j)}$. After traversing all the generated structures, we obtain a matrix $\mathbf{L}^s$ that measures similarity, where the matrix element $\mathbf{L}_{ij} = \exp(-0.5d(i,j)^2)$. The diagonal elements of $\mathbf{L}^s$ are zero because they correspond to the same structure. As a result, we define the final similarity matrix as $\mathbf{L}^p = \mathbf{L}^s + \mathbf{I}$, where $\mathbf{I}$ is an identity matrix. From a mathematical perspective, the determinant of a matrix reflects the range of its data distribution. Therefore, we calculate the $\det(\mathbf{L}^p)$ metric to assess the diversity, with larger values indicating higher diversity in terms of physical properties.

Comparison and discussion. The motivation behind our approach is that current methods focus solely on the geometric properties of structures, whereas incorporating topological features can greatly enhance the diversity in the generation of metamaterial unit structures.

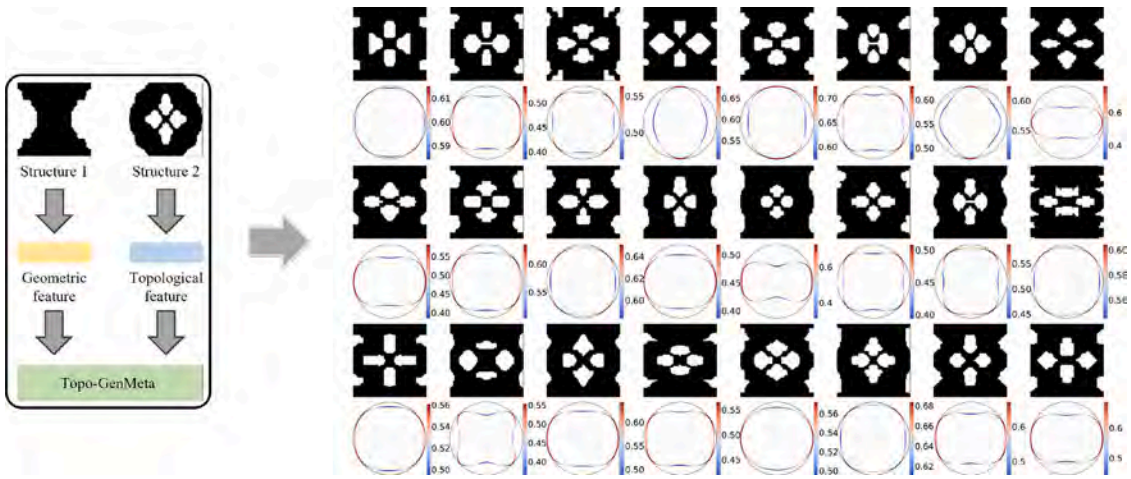

Fig. 9. A series of unit structures generated by our framework under a fixed geometric feature code and a fixed topological feature code.

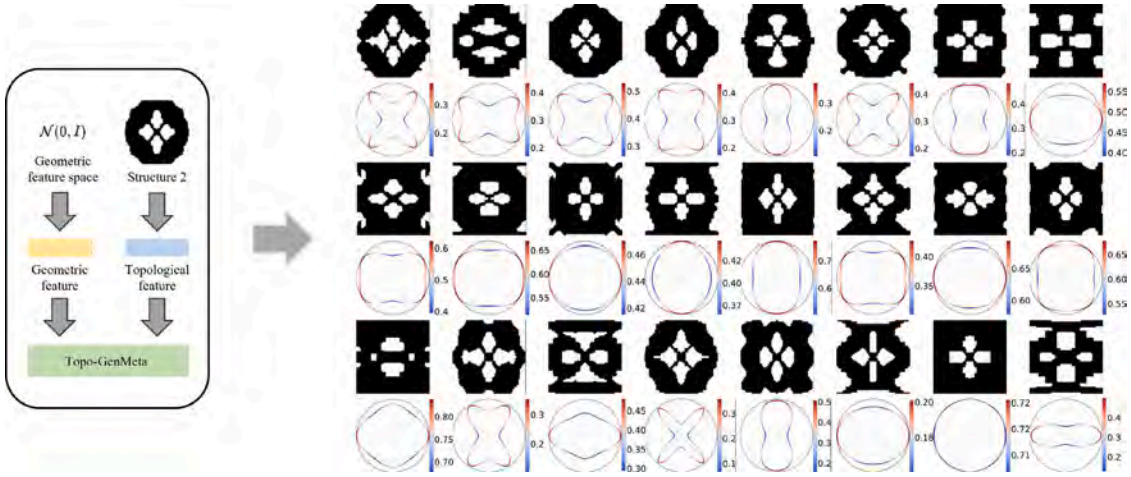

Fig. 10. A series of unit structures generated by our framework under random sampling from the geometric feature space and a fixed topological feature code.

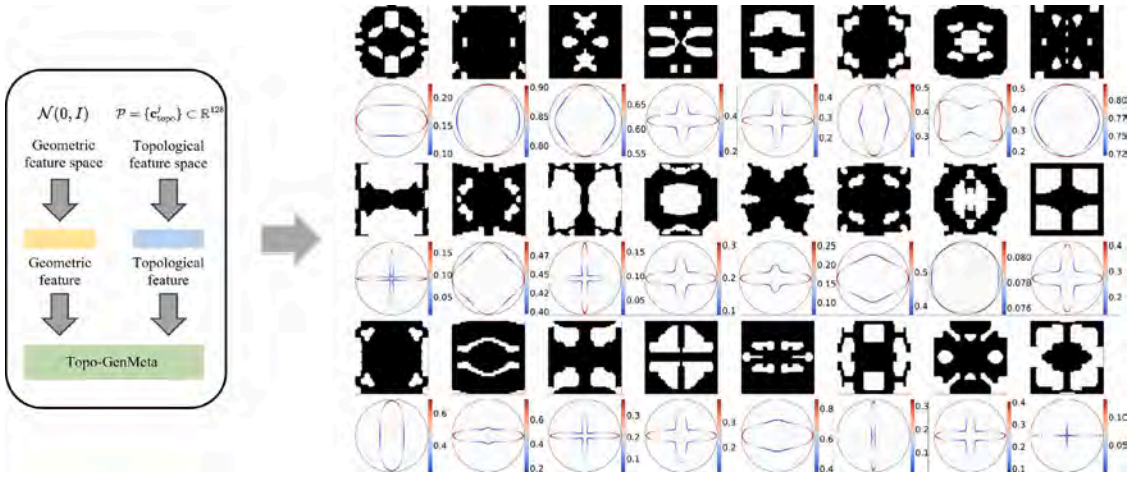

Fig. 11. A series of unit structures generated by our framework under jointly random sampling from both the geometric and the topological feature spaces.

We conduct an ablation study on topological features to illustrate this point. As shown in Table 1, "w/o topo" indicates that topological features are not used as conditional information during the training and generation phases of our Topo-GenMeta model. We employ the same network architecture as depicted in Fig. 4, but we exclude the topological net ϕ_{topo} and the input topological information. It is evident that topological features significantly enhance the diversity of generated structures and also slightly improve their quality.

In our experiments, we produce 1000 unit structures using both our approach and the VAE-based methods to compute the $\det(\mathbf{L}_p)$ metric. Additionally, we perform the generation process 10 times to acquire the average values, as shown in Table 1. Our method achieves the highest

Table 1
Quantity comparison. We compare the P_{FM} and $\det(\mathbf{L}^p)$ metrics across different methods to quantitatively evaluate their performance in terms of quality and physical property diversity in generated unit structures. We also conduct ablation study on topological features, demonstrating that using topological features as conditional input can improve the quality and diversity of the generated structures.

Method	P_{FM} ↓	$\det(\mathbf{L}^p)$ ↑($\times 10^8$)
VAE-Bi	37.78%	7.15
VAE-SDF	10.65%	8.39
GAN-Bi	14.47%	5.13
GAN-SDF	8.00%	5.21
Ours (w/o topo)	3.10%	3.79
Ours (w/ topo)	**2.60%**	**18.72**

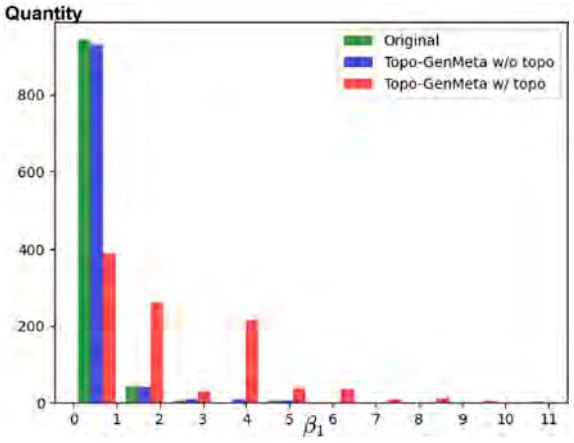

Fig. 12. The comparison between the unit structures in the original dataset and the generated unit structures along the 1-dimensional topological quantity β_1, where β_1 represents the number of holes in each structure. Incorporating topological properties significantly enhances the shape diversity of the generated metamaterial structures.

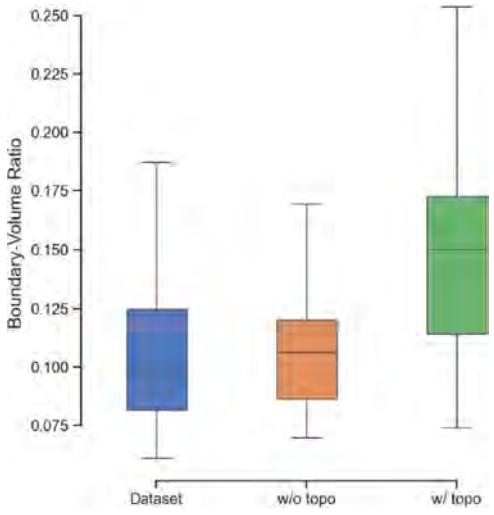

Fig. 13. The distribution comparison between the unit structures in the original dataset and the generated unit structures along the boundary-to-area ratios.

diversity metric compared to previous methods. It is worth noting that the VAE-Bi and VAE-SDF methods often generate structures with significant quality issues, as shown in Fig. 5(a). This somewhat contributes to a rise in the diversity of physical properties; nevertheless, these structures are not practically usable. Similarly, GAN-Bi and GAN-SDF also struggle to produce structurally consistent outputs. While GAN-SDF achieves a relatively low P_{FM} score, many of the generated structures suffer from ambiguous shapes or blended topologies, as illustrated in Fig. 5(b). This ambiguity undermines their practical applicability and limits the diversity gain. Consequently, the metric in Table 1 is higher for VAE-Bi and VAE-SDF than for our framework when topological features are excluded. We stress, however, that our model can boost structural diversity while maintaining high generation quality.

We calculate the quantity of β_1 for the original dataset and the structures generated by our method, both with and without topological guidance. As shown in Fig. 12, our method can generate unit structures with more complex topological features. However, Topo-GenMeta without topological guidance produces a distribution similar to the original dataset, with fewer and more uniform structures containing holes. This strongly demonstrates the effectiveness and significance of the topological module in our method. The statistical results presented here are derived from randomly selecting 1000 samples from each structural dataset.

5.3. The significance of diversity in other applications

It is obvious that the diversity in the shapes of metamaterial unit structures can generate structures with more enriched properties, not only mechanical properties, but also other applications.

Boundary-to-area ratio. In the biomedical field, structures with high surface-to-volume ratios are commonly used as implants. Therefore, we assess property diversity by the boundary-to-area ratio of the unit structures in the 2D case. Specifically, we randomly selected 1000 unit structures from the original dataset and generated an equal number of structures with and without topological guidance for comparison. Fig. 13 shows the distribution of boundary-to-area ratios by box-plots, illustrating that the introduction of topological features markedly increases the diversity of unit structure boundary shapes. This enhancement suggests potential applications in designing cell adhesion growth devices or thermal conduction devices.

Wave propagation. Metamaterials can achieve unique wave propagation properties by controlling the dispersion relation. The dispersion relation plays a critical role across various applications [60–63]. As shown in Fig. 14(a), we conduct numerical simulations using the finite element method (FEM) [63] to calculate the dispersion relations of unit structures. The obtained dispersion relation is represented as a 10×30 eigenfrequency matrix, which is then reduced to three dimensions using PCA for visualization. We randomly selected 500 unit structures from the original dataset and generated an equal number of structures with and without topological guidance. We visualize the dimensionally reduced dispersion relation features in a 3D coordinate space, as shown in Fig. 14(b–d). The color in (c–d) represents the distance to the nearest point in the original dataset (b). It demonstrates that the inclusion of topological features significantly enhances the diversity of dispersion relations in the generated unit structures.

Negative Poisson's ratio. Negative Poisson's ratio property is an important goal in metamaterial design. Its unconventional mechanical behavior, such as lateral expansion under axial tension, provides significant advantages in energy absorption and impact resistance. To evaluate the effectiveness of our method in NPR metamaterial design, we first construct a sample set, denoted as S_o, comprising unit structures with negative Poisson's ratios from the original dataset, along with their physical properties and PIs. We then encode these PIs into a latent space using the trained topological encoder, as introduced in Section 4.2.2. Next, we generate a sample set, denoted as S_g, using the method illustrated in Fig. 11. As shown in Fig. 15, we visualize the distribution of S_o and S_g in the Young's modulus-Poisson's ratio space to quantify and analyze the model's generative capability. According to our statistics, only 0.57% of our training dataset exhibit a negative Poisson's ratio. However, by leveraging topological features corresponding to unit structures with negative Poisson's ratio, our

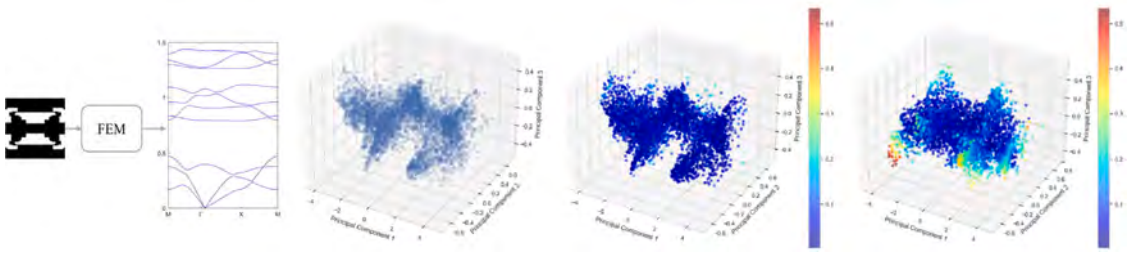

(a) dispersion relation (b) dataset (c) w/o topo (d) w/ topo

Fig. 14. We conduct finite element method to obtain the dispersion relation for a unit structure. Then we perform dimensionality reduction on all relationship vectors and visualize their distribution, which indicate the unit structures in the training dataset, structures generated without topology information, and structures generated with topology information, respectively.

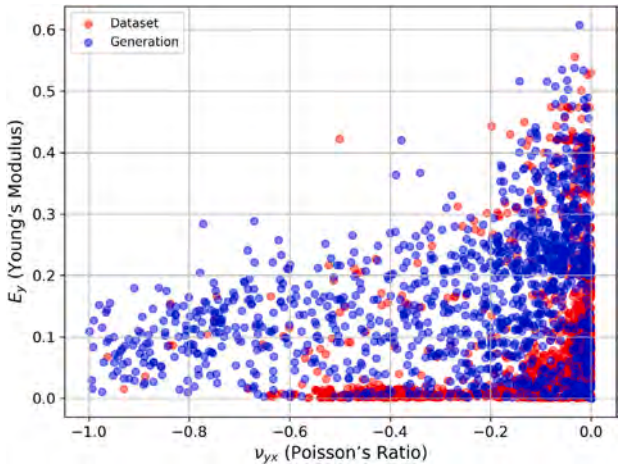

Fig. 15. Visualization of Poisson's ratio values and corresponding Young's modulus scatter plots for negative Poisson's ratio structures in the training dataset. By incorporating topological feature guidance, our method is capable of generating negative Poisson's ratio structures with a broader range of mechanical properties.

method significantly enhances the generation of negative Poisson's ratio structures, as shown in Fig. 15, where the generated samples effectively cover and fill the entire distribution. This experiment also suggests that structures with the same target properties may share certain topological similarities, which inspires future research to further clarify their intrinsic relationships.

Note. We want to emphasize that this paper primarily focuses on proposing a topology-aware framework for generating metamaterial unit structures. This framework possesses the ability to create diverse, high-quality metamaterial unit structures, which is comprehensively demonstrated by the experiments presented above. This capacity is crucial for expanding the metamaterial unit library, offering a broader range of options to suit various application needs, which is indeed the main objective of this section. We also clarify that dynamic properties are not explicitly modeled in this section, and the results are only intended to demonstrate the potential of our framework to generate structures with diverse dynamic properties. Although exploring the exact relationships among structure, topology, and properties is certainly interesting and significant, it remains a highly challenging task that extends beyond the scope of this paper. We will explore this issue further in future work.

5.4. Target deformation problem

For a beam with Height = 5 and Width = 20, we aim to achieve a specified target deformation under given boundary conditions by designing the internal filling with metamaterial unit structures. Following the 2D adaptation of the framework by Wang et al. [64], the topology optimization problem is formulated as:

$$\begin{aligned} \text{minimize} \quad & I_d = (\mathbf{u}-\hat{\mathbf{u}})^T \mathbf{D}(\mathbf{u}-\hat{\mathbf{u}}), \\ \text{subject to} \quad & \mathbf{K}(C_i)\mathbf{u} = \mathbf{f}, \\ & \boldsymbol{\Phi}(C_i) \le 0, \quad i = 1, \dots, N_e. \end{aligned} \tag{8}$$

Here, C_i denotes the four independent components of the elastic tensor $(C_{11}, C_{12}, C_{22}, C_{33})$. $\hat{\mathbf{u}}$ is the target displacement vector, $\mathbf{D}$ specifies the query nodes of interest. $\mathbf{K}$ is the global stiffness matrix, $\mathbf{u}$ is the displacement vector, and $\mathbf{f}$ is the external loads applied to the object. The inequality constraint $\boldsymbol{\Phi} \le 0$ ensures that the properties of each unit structure remain within the range of the data distribution. N_e denotes the total number of unit cells. The configuration of the design problem is given in Fig. 16(a), and the design domain is discretized into 100 elements. We fix the left side of the beam and constrain the vertical displacement on the right side, then compress the right side to a horizontal displacement. In addition, the yellow dashed line indicates the target deformation location of interest. To this end, we conducted two experiments to fit the deformation in the curves depicted in Fig. 16(b) and (c). In our implementation, we adopt a heuristic strategy. First, the target property of each unit cell is determined by topology optimization. Next, we generate multiple unit structures that meet the target properties as candidates. Finally, from these candidates, we select metamaterial structures that guarantee overlap between adjacent unit cells for infilling. It should be noted that the effectiveness of this heuristic approach is primarily due to the ability of our method to generate unit metamaterial structures that are high quality, diverse and exhibit high property fidelity. The resulting structures generated by our method are presented in Fig. 16(d) and (e). After simulation of finite elements, the displacement at the bottom of the beam precisely matches the design targets, with a mean square error (MSE) of 0.00329 and 0.00003, respectively. To reflect real-world conditions, the simulation base material is selected as a flexible material, as shown in Fig. 16(f) and (g).

6. Conclusion and future work

In this paper, we introduce a novel topology-aware metamaterial unit structures generative model, *Topo-GenMeta*. Our framework combines persistent homology techniques with the denoising diffusion probabilistic model, successfully decomposing the geometric and topological feature space of metamaterial unit structures for learning. This enables our model to generate metamaterial unit structures with various geometric and topological variations. Extensive experimental results demonstrate that the unit structures generated by our framework exhibit superior performance in both quality and diversity. Furthermore, our model has also been verified to be effectively applicable to the design of multi-scale structures. Our model is capable of producing numerous high-quality metamaterial unit structures with

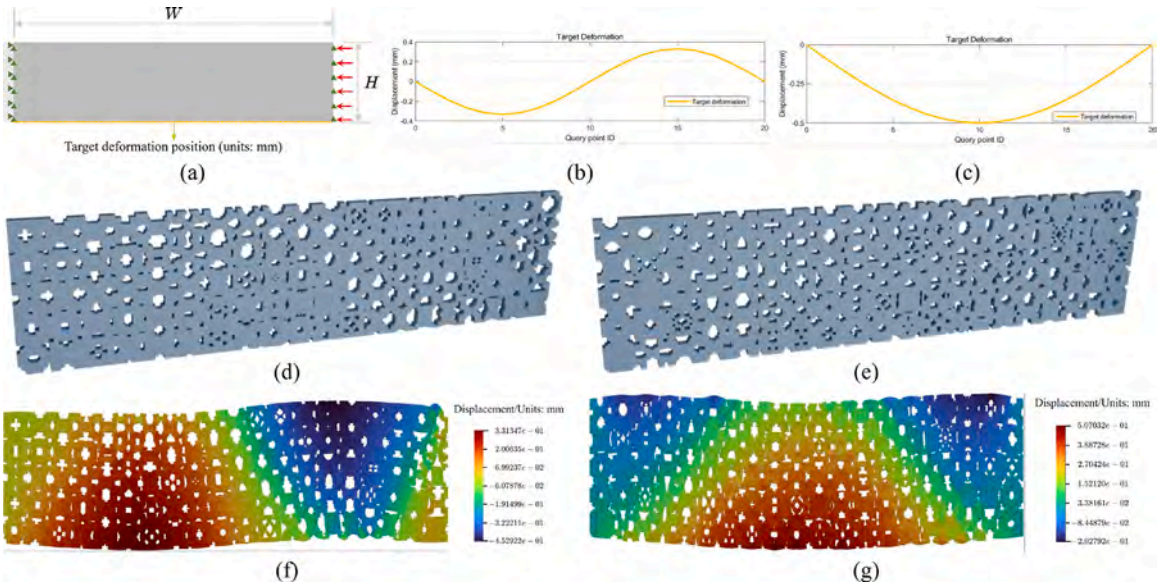

Fig. 16. Application of the Topo-GenMeta framework to design multi-scale structures to achieve target deformation.

diverse properties, which effectively expands existing metamaterial library and act as a standard for future studies in this domain.

To further enhance the practicality of our approach, we aim to extend Topo-GenMeta to 3D metamaterials. Several key challenges require further investigation. First, generating voxel-based 3D unit structure datasets entails substantial computational time and memory consumption. Future research could focus on optimizing the trade-off between dataset scale and construction cost. Second, while diffusion models outperform other generative approaches in producing high-quality unit structures, their training remains computationally intensive. Given the significantly higher complexity of 3D scenarios compared to 2D, developing more efficient generative models is a critical direction for future work.

CRediT authorship contribution statement

Liang Du: Writing – original draft, Methodology, Investigation. **Jiangbei Hu:** Writing – review & editing, Methodology, Investigation. **Shengfa Wang:** Writing – review & editing, Supervision, Project administration, Methodology. **Yu Jiang:** Visualization, Formal analysis. **Na Lei:** Validation, Funding acquisition. **Ying He:** Writing – review & editing, Validation. **Zhongxuan Luo:** Writing – review & editing, Funding acquisition.

Declaration of competing interest

The authors declare that they have no known competing financial interests or personal relationships that could have appeared to influence the work reported in this paper.

Acknowledgments

We thank the anonymous reviewers for their constructive feedback. Part of this work was conducted while the leading author (J. Hu) was with NTU. This research was mainly supported by the National Natural Science Foundation of No. 62402083. In addition, the work was partly supported by the National Key R&D Program of China (2021YFA1003003, 2023YFB3309102), the National Natural Science Foundation of China (T2225012, 12494550, 12494554), Fundamental Research Funds for the Central Universities, China (DUT25RC(3)031), Dalian Science and Technology Talent Innovation Support Program (2022RG04), the Ministry of Education, Singapore, under its Academic Research Fund Grant (RT19/22).

Data availability

Data will be made available on request.

References

[1] Zheludev NI, Kivshar YS. From metamaterials to metadevices. Nat Mater 2012;11(11):917–24.
[2] Engheta N, Ziolkowski RW. Metamaterials: physics and engineering explorations. John Wiley & Sons; 2006.
[3] Apaydin N, Sertel K, Volakis JL. Nonreciprocal and magnetically scanned miniaturized leaky-wave antennas using coupled transmission lines. EPJ Appl Metamaterials 2014;1:3.
[4] Hu G, Tang L, Banerjee A, Das R. Metastructure with piezoelectric element for simultaneous vibration suppression and energy harvesting. J Vib Acoust 2017;139(1):011012.
[5] Kumar R, Kumar M, Chohan JS, Kumar S. Overview on metamaterial: History, types and applications. Mater Today: Proc 2022;56:3016–24.
[6] Hussein MI, Leamy MJ, Ruzzene M. Dynamics of phononic materials and structures: Historical origins, recent progress, and future outlook. Appl Mech Rev 2014;66(4):040802.
[7] Askari M, Hutchins DA, Thomas PJ, Astolfi L, Watson RL, Abdi M, et al. Additive manufacturing of metamaterials: A review. Addit Manuf 2020;36:101562.
[8] Fan J, Zhang L, Wei S, Zhang Z, Choi S-K, Song B, et al. A review of additive manufacturing of metamaterials and developing trends. Mater Today 2021;50:303–28.
[9] Li H, Luo Z, Gao L, Walker P. Topology optimization for functionally graded cellular composites with metamaterials by level sets. Comput Methods Appl Mech Engrg 2018;328:340–64.
[10] Kumar S, Tan S, Zheng L, Kochmann DM. Inverse-designed spinodoid metamaterials. Npj Comput Mater 2020;6(1):73.
[11] Song J, Lee J, Kim N, Min K. Artificial intelligence in the design of innovative metamaterials: A comprehensive review. Int J Precis Eng Manuf 2024;25(1):225–44.
[12] Qian C, Kaminer I, Chen H. A guidance to intelligent metamaterials and metamaterials intelligence. Nat Commun 2025;16(1):1154.
[13] Lee D, Chen W, Wang L, Chan Y-C, Chen W. Data-driven design for metamaterials and multiscale systems: A review. Adv Mater 2023;2305254.
[14] Wang L, Chan Y-C, Ahmed F, Liu Z, Zhu P, Chen W. Deep generative modeling for mechanistic-based learning and design of metamaterial systems. Comput Methods Appl Mech Engrg 2020;372:113377.
[15] Lee D, Chan Y-C, Chen W, Wang L, van Beek A, Chen W. T-METASET: Task-aware acquisition of metamaterial datasets through diversity-based active learning. J Mech Des 2023;145(3):031704.
[16] Zheng X, Chen T-T, Guo X, Samitsu S, Watanabe I. Controllable inverse design of auxetic metamaterials using deep learning. Mater Des 2021;211:110178.
[17] Kollmann HT, Abueidda DW, Koric S, Guleryuz E, Sobh NA. Deep learning for topology optimization of 2D metamaterials. Mater Des 2020;196:109098.

[18] Wilt JK, Yang C, Gu GX. Accelerating auxetic metamaterial design with deep learning. Adv Eng Mater 2020;22(5):1901266.

[19] Jiang X, Liu F, Wang L. Machine learning-based stiffness optimization of digital composite metamaterials with desired positive or negative Poisson's ratio. Theor Appl Mech Lett 2023;13(6):100485.

[20] Zheng L, Karapiperis K, Kumar S, Kochmann DM. Unifying the design space and optimizing linear and nonlinear truss metamaterials by generative modeling. Nat Commun 2023;14(1):7563.

[21] Bastek J-H, Kumar S, Telgen B, Glaesener RN, Kochmann DM. Inverting the structure–property map of truss metamaterials by deep learning. Proc Natl Acad Sci 2022;119(1):e2111505119.

[22] Zeng Q, Zhao Z, Lei H, Wang P. A deep learning approach for inverse design of gradient mechanical metamaterials. Int J Mech Sci 2023;240:107920.

[23] Bastek J-H, Kochmann DM. Inverse-design of nonlinear mechanical metamaterials via video denoising diffusion models. 2023, arXiv preprint arXiv:2305.19836.

[24] Wang H, Du Z, Feng F, Kang Z, Tang S, Guo X. DiffMat: Data-driven inverse design of energy-absorbing metamaterials using diffusion model. Comput Methods Appl Mech Engrg 2024;432:117440.

[25] Felsch G, Ghavidelnia N, Schwarz D, Slesarenko V. Controlling auxeticity in curved-beam metamaterials via a deep generative model. Comput Methods Appl Mech Engrg 2023;410:116032.

[26] Chan Y-C, Ahmed F, Wang L, Chen W. METASET: Exploring shape and property spaces for data-driven metamaterials design. J Mech Des 2021;143(3):031707.

[27] Feng J, Wang L, Zhai X, Chen K, Wu W, Liu L, et al. Constructing boundary-identical microstructures via guided diffusion for fast multiscale topology optimization. Comput Methods Appl Mech Engrg 2025;436:117735.

[28] Kegl M, Brank B. Shape optimization of truss-stiffened shell structures with variable thickness. Comput Methods Appl Mech Engrg 2006;195(19):2611–34.

[29] Liang Y, Yan X, Cheng G. Explicit control of 2D and 3D structural complexity by discrete variable topology optimization method. Comput Methods Appl Mech Engrg 2022;389:114302.

[30] Zhou L, Gao T, Zhang W. Hole control methods in feature-driven topology optimization. Comput Methods Appl Mech Engrg 2023;417:116447.

[31] Edelsbrunner H, Harer J, et al. Persistent homology-a survey. Contemp Math 2008;453(26):257–82.

[32] Otter N, Porter MA, Tillmann U, Grindrod P, Harrington HA. A roadmap for the computation of persistent homology. EPJ Data Sci 2017;6:1–38.

[33] Obayashi I, Nakamura T, Hiraoka Y. Persistent homology analysis for materials research and persistent homology software: HomCloud. J Phys Soc Japan 2022;91(9):091013.

[34] Clough JR, Byrne N, Oksuz I, Zimmer VA, Schnabel JA, King AP. A topological loss function for deep-learning based image segmentation using persistent homology. IEEE Trans Pattern Anal Mach Intell 2020;44(12):8766–78.

[35] Muñoz D, Allix O, Chinesta F, Ródenas J, Nadal E. Manifold learning for coherent design interpolation based on geometrical and topological descriptors. Comput Methods Appl Mech Engrg 2023;405:115859.

[36] Townsend J, Micucci CP, Hymel JH, Maroulas V, Vogiatzis KD. Representation of molecular structures with persistent homology for machine learning applications in chemistry. Nat Commun 2020;11(1):3230.

[37] Moor M, Horn M, Rieck B, Borgwardt K. Topological autoencoders. In: International conference on machine learning. PMLR; 2020, p. 7045–54.

[38] Xia K, Wei G-W. Persistent homology analysis of protein structure, flexibility, and folding. Int J Numer Methods Biomed Eng 2014;30(8):814–44.

[39] Vipond O, Bull JA, Macklin PS, Tillmann U, Pugh CW, Byrne HM, et al. Multiparameter persistent homology landscapes identify immune cell spatial patterns in tumors. Proc Natl Acad Sci 2021;118(41):e2102166118.

[40] Qiu Y, Wei G-W. Persistent spectral theory-guided protein engineering. Nat Comput Sci 2023;3(2):149–63.

[41] Zhou C, Dong Z, Lin H. Learning persistent homology of 3D point clouds. Comput Graph 2022.

[42] Dong Z, Chen J, Lin H. Topology-controllable implicit surface reconstruction based on persistent homology. Computer-Aided Des 2022;150:103308.

[43] He Z, Zhuo P, Lin H, Dai J. 3D shape descriptor design based on HKS and persistent homology with stability analysis. Comput Aided Geom Design 2024;111:102326.

[44] Pun CS, Lee SX, Xia K. Persistent-homology-based machine learning: a survey and a comparative study. Artif Intell Rev 2022;55(7):5169–213.

[45] Bubenik P, et al. Statistical topological data analysis using persistence landscapes.. J Mach Learn Res 2015;16(1):77–102.

[46] Umeda Y. Time series classification via topological data analysis. Inf Media Technol 2017;12:228–39.

[47] Adams H, Emerson T, Kirby M, Neville R, Peterson C, Shipman P, et al. Persistence images: A stable vector representation of persistent homology. J Mach Learn Res 2017;18.

[48] Gao D, Zhang Y, Lin H, Zou Q. Persistent homology-driven optimization of effective relative density range for triply periodic minimal surfaces. Computer-Aided Des 2025;180:103835.

[49] Zhuo P, He Z, Lin H. Persistent geometry-topology descriptor for porous structure retrieval based on heat kernel signature. Graph Model 2024;133:101219.

[50] Behzadi MM, Ilieş HT. Gantl: Toward practical and real-time topology optimization with conditional generative adversarial networks and transfer learning. J Mech Des 2022;144(2):021711.

[51] Hu J, He Y, Xu B, Wang S, Lei N, Luo Z. IF-TONIR: Iteration-free topology optimization based on implicit neural representations. Computer-Aided Des 2024;167:103639.

[52] Ho J, Jain A, Abbeel P. Denoising diffusion probabilistic models. Adv Neural Inf Process Syst 2020;33:6840–51.

[53] Wagner H, Chen C, Vuçini E. Efficient computation of persistent homology for cubical data. In: Topological methods in data analysis and visualization II: theory, algorithms, and applications. Springer; 2011, p. 91–106.

[54] Bleile B, Garin A, Heiss T, Maggs K, Robins V. The persistent homology of dual digital image constructions. In: Research in computational topology 2. Springer; 2022, p. 1–26.

[55] Dong G, Tang Y, Zhao YF. A 149 line homogenization code for three-dimensional cellular materials written in matlab. J Eng Mater Technol 2019;141(1):011005.

[56] Yalameha S, Nourbakhsh Z, Vashaee D. ElATools: A tool for analyzing anisotropic elastic properties of the 2d and 3D materials. Comput Phys Comm 2022;271:108195.

[57] Maria C, Boissonnat J-D, Glisse M, Yvinec M. The gudhi library: Simplicial complexes and persistent homology. In: Mathematical software–ICMS 2014: 4th international congress, Seoul, South Korea, August 5-9, 2014. proceedings 4. Springer; 2014, p. 167–74.

[58] Mildenhall B, Srinivasan PP, Tancik M, Barron JT, Ramamoorthi R, Ng R. Nerf: Representing scenes as neural radiance fields for view synthesis. Commun ACM 2021;65(1):99–106.

[59] Song J, Meng C, Ermon S. Denoising diffusion implicit models. 2020, arXiv preprint arXiv:2010.02502.

[60] Ma G, Fu C, Wang G, Del Hougne P, Christensen J, Lai Y, et al. Polarization bandgaps and fluid-like elasticity in fully solid elastic metamaterials. Nat Commun 2016;7(1):13536.

[61] Gliozzi AS, Miniaci M, Chiappone A, Bergamini A, Morin B, Descrovi E. Tunable photo-responsive elastic metamaterials. Nat Commun 2020;11(1):2576.

[62] Chen Y, Kadic M, Wegener M. Roton-like acoustical dispersion relations in 3D metamaterials. Nat Commun 2021;12(1):3278.

[63] Jiang W, Zhu Y, Yin G, Lu H, Xie L, Yin M. Dispersion relation prediction and structure inverse design of elastic metamaterials via deep learning. Mater Today Phys 2022;22:100616.

[64] Wang J, Chen WW, Da D, Fuge M, Rai R. IH-GAN: A conditional generative model for implicit surface-based inverse design of cellular structures. Comput Methods Appl Mech Engrg 2022;396:115060.